FREE VIBRATIONS OF THIN-WALLED SEMICIRCULAR GRAPHITE-EPOXY COMPOSITE FRAMES

Huey D. Carden*
NASA Langley Research Center
Hampton, VA

Ahmed K. Noor** and Jeanne M. Peters†
George Washington University
NASA Langley Research Cener
Hampton, VA

Abstract

A detailed study is made of the effects of variations in lamination and material parameters of thin-walled composite frames on their vibrational characteristics. The structures considered are semicircular thin-walled frames with I and J sections. The flanges and webs of the frames are modeled by using two-dimensional shell and plate finite elements. A mixed formulation is used with the fundamental unknowns consisting of both the generalized displacements and stress resultants in the frame. The frequencies and modes predicted by the two-dimensional finite element model are compared with those obtained from experiments, as well as with the predictions of a one-dimensional thin-walled beam finite element model. A detailed study is made of the sensitivity of the vibrational response to variations in the fiber orientation, material properties of the individual layers, and boundary conditions.

Introduction

The physical understanding and the numerical simulation of the dynamic response of laminated anisotropic structures have recently become the focus of intense efforts because of the expanded use of fibrous composites in aerospace, automotive, shipbuilding, and other industries, and the need to establish the practical limits of the dynamic load-carrying capability of structures made from these materials. References 1-45 are indicative of the general interest and efforts focused on various aspects of the vibration of structures. Experimental studies have been performed on the free vibration and impact-response of thin-walled composite frames and stiffeners.[1-4] One-dimensional theories have been developed for the static, vibration and buckling analyses of thin-walled frame structures.[5-8] However, no systematic assessment has been made of the range of validity of the basic assumptions of these theories. Approximate analytical and numerical techniques have been applied to the study of the vibrational response of isotropic and composite stiffeners.[9-21] Only a few publications[22-23] examine the effects of variations in lamination and geometric parameters of composite panels on their vibrational characteristics, and these publications do not consider thin-walled composite frames.

The present study summarizes the results of a recent study (Noor, Carden, Peters)[24] on the effects of variations in the lamination and geometric parameters of thin-walled composite frames on their vibrational characteristics (frequencies, and energy components associated with different modes). The frames considered are semicircular, made of thin-walled graphite-epoxy material with I and J sections and have a 36-inch radius (see Fig. 1).

Analysis

Computational Models

Two computational models are used for the thin-walled composite frames study. In the first model, the flanges and web are modeled using two-dimensional shell and plate finite elements. The second model is a finite element discretization of the one-dimensional Vlasov's type thin-walled beam theory. Henceforth, the two models will be referred to as two-dimensional (2D) and one-dimensional (1D) finite element models, respectively.

Mathematical Formulation

a) Two-dimensional models. The analytical formulation for the two-dimensional models is based on the Sanders-Budiansky shell theory with the effects of transverse shear deformation, and laminated anisotropic material response included. A mixed formulation is used with the fundamental unknowns consisting of both the generalized displacements and the stress resultants in the frame (see Fig. 2 for the sign convention).

Bicubic shape functions are used to approximate each of the generalized displacements and the stress resultants. The number of displacement nodes in each element is 16. The stress resultants are allowed to be discontinuous at interelement boundaries. The total number of stress-resultant parameters in each element is 128. The element characteristic arrays are obtained by using the two-field Hellinger-Reissner mixed variational principle.

*Assistant Head, Landing and Impact Dynamics Branch
**Professor of Engineering and Applied Science
†Programmer Analyst

b) One-dimensional models. The analytical formulation for one-dimensional models is based on a form of Vlasov's thin-walled beam theory with the effects of flexural-torsional coupling, transverse shear deformation, and rotary inertia included. The fundamental unknowns consist of seven internal forces and seven generalized displacements of the beam (see Fig. 3 for the sign convention). The element characteristic arrays are obtained by using a modified form of the Hellinger-Reissner mixed variational principle. The modification consists of augmenting the functional of that principle by two terms: 1) the Lagrange multiplier associated with the constraint condition relating the rotation of the cross section and the twist degrees of freedom; and 2) a regularization term that is quadratic in the Lagrange multiplier. Only C^0 continuity is required for the generalized displacements. Lagrangian interpolation functions are used for approximating each of the generalized displacements, internal forces and Lagrange multiplier. The polynomial functions for the internal forces and the Lagrange multiplier are one degree lower than those of the generalized displacements. In the present study quadratic polynomials are used in approximating the generalized displacements. Linear polynomials are used in approximating each of the internal forces and the Lagrange multiplier. The internal forces and the Lagrange multiplier are allowed to be discontinuous at interelement boundaries. For each element the total number of generalized displacement parameters is 21, the total number of internal force parameters is 14 and the total number of Lagrange multiplier parameters is 2. Noor, Peters and Min[25] present the fundamental equations of the thin-walled beam theory.

For quasi-isotropic laminated composites, numerical experiments to be described subsequently have demonstrated that reasonably accurate results can be obtained using the one-dimensional model when the laminated composite is replaced by an equivalent isotropic material with the following Young's and shear moduli:

$$E = A_{11}/h \tag{1}$$

$$G = A_{33}/h \tag{2}$$

where A_{11} and A_{33} are the extensional stiffness in the x direction, and the in-plane shear stiffness used in the classical lamination theory, respectively; and h is the total wall thickness (of the flange or web). This approximation was adopted in the present study.

Finite Element Equations

The finite element equations for each individual element of the 1D and 2D models can be cast in the following compact form:

$$\left(\overset{*}{[K]} - \omega^2 \overset{*}{[M]}\right)\{Z\} = 0 \tag{3}$$

where $\{Z\}$ is the vector of the element degrees of freedom; ω is the frequency of vibration; $\overset{*}{[K]}$ and $\overset{*}{[M]}$ are the generalized stiffness and mass matrices. The explicit forms of matrix arrays associated with $\{Z\}$, $\overset{*}{[K]}$ and $\overset{*}{[M]}$ are given in Noor and Anderson[26], and Noor and Peters[27] for the two-dimensional models, and Noor, et al[25] for the one-dimensional model.

Vibrational Sensitivity to Variations in Lamination and Material Parameters

The expressions for the sensitivity derivatives of the frequency and response vector with respect to the lamination and material parameters, λ_i, of the composite frames are given by:[28]

$$\frac{\partial\omega^2}{\partial\lambda_i} = \sum_{\text{elements}} \{Z\}^t \left(\frac{\partial \overset{*}{[K]}}{\partial\lambda_i} - \omega^2 \frac{\partial \overset{*}{[M]}}{\partial\lambda_i} \right)\{Z\} \tag{4}$$

and

$$\frac{\partial\{Z\}}{\partial\lambda_i} = \overset{*}{\{Z\}} + c_i \{Z\} \tag{5}$$

where $\overset{*}{\{Z\}}$ represents a particular solution of the equations:

$$\left(\overset{*}{[K]} - \omega^2 \overset{*}{[M]}\right)\frac{\partial\{Z\}}{\partial\lambda_i} = -\left(\frac{\partial \overset{*}{[K]}}{\partial\lambda_i} - \omega^2 \frac{\partial \overset{*}{[M]}}{\partial\lambda_i} - \frac{\partial\omega^2}{\partial\lambda_i} \overset{*}{[M]} \right)\{Z\} \tag{6}$$

and c_i are multipliers given by:

$$c_i = -\sum_{\text{elements}} \left(\overset{*}{\{Z\}}^t [M]\{Z\} + \{Z\}^t \left[\frac{\partial M}{\partial\lambda_i}\right]\{Z\} \right) \tag{7}$$

In Eqs. 4 to 7, the eigenvectors are assumed to be normalized with respect to $\overset{*}{[M]}$, i.e.

$$\{Z\}^t \overset{*}{[M]} \{Z\} = 1 \tag{8}$$

The expressions for the total complementary strain energy of the frame, U^c, and its derivatives with respect to λ_i, are given by:

$$U^c = \frac{1}{2} \sum_{\text{elements}} \{H\}^t [F] \{H\} \tag{9}$$

and

$$\frac{\partial U^c}{\partial\lambda_i} = \sum_{\text{elements}} \left(\frac{1}{2} \{H\}^t \frac{\partial [F]}{\partial\lambda_i} \{H\} + \left\{\frac{\partial H}{\partial\lambda_i}\right\}^t [F]\{H\} \right) \tag{10}$$

For the purpose of obtaining analytic derivatives with respect to some of the lamination parameters, such as the fiber orientation angle of different layers, it is convenient to express $\frac{\partial[F]}{\partial\lambda_i}$ in terms of $\frac{\partial[F]^{-1}}{\partial\lambda_i}$ as follows:

$$\frac{\partial[F]}{\partial\lambda_i} = -[F] \frac{\partial[F]^{-1}}{\partial\lambda_i} [F] \tag{11}$$

The matrix $\frac{\partial[F]^{-1}}{\partial\lambda_i}$ is evaluated using the analytical derivatives of the material stiffness matrix of each laminate (flanges and

web). The material stiffness matrix of the laminate is given in Jones.[29]

Experimental and Numerical Studies

Apparatus and Test Procedure

a. *Specimens.* Two specimens, shown in Fig. 4, were tested, an I-section and a J-section frame. Nominal dimensions of each cross section are shown in Fig. 1. Weight of the frame sections was 3.181 and 4.085 lb. (1.443 and 1.853 kg) for the I and J frames, respectively. The frame sections were made from AS4/5208 graphite/epoxy unidirectional tape layed up in a manner which resulted in essentially uniform stiffness properties in the circumferential direction (i.e., the stiffness coefficients are independent of $\bar{\theta}$). The material properties for the individual layers are given in Fig. 1. The laminate stacking sequence for the I-section was $|\pm 45/0/90|_s$ and $|\pm 45/0/90|_{2s}$ for the J-section. Each frame section was semicircular with a diameter of 72 inches (1.8288 m.). Bonded to the outside flange of each frame was a sixteen-ply $|\pm 45/0/90|_{2s}$, quasi-isotropic skin made of the same material. The frame sections were constructed so that the skin would extend 0.5 inches (0.0127 m.) beyond each side of the bottom flange of the frame. Measured dimensions were used in one of the finite-element models and results were compared to nominal dimension results and the experimental data.

b. *Instrumentation and test method.* A photograph of the test equipment and composite frame specimens is shown in Fig. 4. The ends of the frame sections were potted in a fixture which was bolted to a large steel beam backstop.

An air-shaker, connected to an air compressor, was used to excite all test specimens. Excitation was both in-plane (radially), and out-of-plane. For in-plane excitation, the shaker was positioned so that the pulses of air struck approximately along a normal to the surface of the skin. For out-of-plane excitation, a piece of styrofoam was attached to the side of the frame by double-sided adhesive tape. Pulses of air struck the flat face of the styrofoam along a normal to the face. The position of the air-shaker was adjusted if the excitation was striking on a node.

A miniature accelerometer was attached at a fixed location to the frame sections with double-sided adhesive tape. Output from the accelerometer was amplified and displayed along the vertical axis of an oscilloscope. Natural modes were determined by tuning the excitation frequency of the air-shaker to produce an acceleration maximum on the vertical deflection on the oscilloscope. Output also passed through a low pass filter and was displayed as vibrational frequency on a frequency counter.

A handheld velocity probe was moved along the frame to determine node locations and mode shapes. The output of the probe was displayed along the horizontal axis of the oscilloscope. The probe and accelerometer outputs combined to create a Lissajous pattern on the oscilloscope. A phase shift in the Lissajous pattern occurred when the velocity probe passed over a node.

Since manual equipment was used in mapping the nodal locations during the vibration survey of the frames, only nodal lines associated with gross in-plane, and gross out-of-plane motions were monitored. Other nodal lines, associated with localized deformation patterns were not surveyed. These localized deformations were noticeable in some of the higher vibration modes, with complex deformation patterns and/or strong coupling between in-plane and out-of-plane motions.

Finite-Element Grids

Two-dimensional models were generated for the actual frames (test specimens) described in the preceding subsection, as well as for the corresponding frames with nominal dimensions. Henceforth, the frames with actual and nominal dimensions will be referred to as the actual and nominal frames, respectively. For the actual frames, spline interpolations through measured dimensions were used to generate the wall thicknesses and coordinates of the nodal points. Isoparametric finite elements were used to approximate the variations in stiffnesses and geometry. The one-dimensional models considered herein are for the frames with nominal dimensions. The grids used for both the one-dimensional and two-dimensional models are described subsequently.

Two-dimensional models. An 18×8 grid was used for modeling the whole I-section frame. In this grid two elements were used to model each of the web, top and bottom flange sections. The part of the skin adjacent to the bottom flange section was treated as part of the flange. One element was used to model each of the two parts of the skin section extending beyond the bottom flange (see Fig. 1). The middle surfaces of the top flange and the web were taken to be their reference surfaces. The middle surface of the combined bottom flange and skin was taken to be the reference surface.

An 18×7 grid was used for modeling the whole J-section frame. The distribution of the elements was similar to the I-section frame. Only one element was used to model the top flange section (see Fig. 1).

Totally clamped and partially clamped support conditions were considered. For totally clamped supports, all the six generalized displacements were restrained $\left(u_1'=u_2'=w'=\phi_1'=\phi_2'=\phi_3'=0\right)$. The partially clamped conditions were obtained from the totally clamped case by successively removing the restraints on one, as well as on combinations, of the displacement and rotation components.

One-dimensional models. A uniform grid of 24 elements was used in modeling each of the I-section and J-section frames. The principal sectorial properties of the cross section were evaluated using the Fortran program listed in Coyette.[30]

Identification of Modes and Estimation of the Error in the One-Dimensional Model Predictions

The two-dimensional models can be used to: a) identify the in-plane, out-of-plane and coupled modes, and b) estimate the error in the predictions of the one-dimensional models. This is accomplished through decomposing the complementary

strain energy, U^c, Eqs. 9, associated with each vibration mode, into three components, U_1, U_2 and U_3 (see Table 1). The first two components, U_1 and U_2 are associated with the in-plane and out-of-plane stress resultants, respectively. The third component, U_3, is associated with the stress resultants which are particular to two-dimensional plates and shells (not present in one-dimensional beam models). The in-plane and out-of-plane modes correspond to the modes for which U_1/U^c and U_2/U^c are close to 1, respectively. The strongly coupled modes correspond to nearly equal values of U_1/U^c and U_2/U^c. The ratio U_3/U^c is indicative of the error in the one-dimensional model predictions.

It is also useful to partition the total complementary strain energy, associated with each mode, into three components, U_{tf}, U_w, U_{bf} representing the contributions of the top flange, web, and bottom flange (including the skin).

Comparison of Experimental and Finite-Element Results

The results of the experimental and numerical studies are summarized in Figs. 5 through 9 and Table 2 for the I-section frame, and in Figs. 10 through 14 and Table 3 for the J-section frame. For the finite element model three cases are considered, namely, totally clamped edges (with both translational and rotational restraints), partially clamped edges with ϕ_2' not restrained, and partially clamped edges (with u_1' in the flanges and ϕ_2' not restrained).

The maximum and minimum values of the frequencies obtained by the two-dimensional finite element model (corresponding to the totally clamped and partially clamped edges) are shown in Figs. 5(a) and 10(a) along with the experimental frequencies. (See also Tables 2 and 3). Note that the experimental frequencies associated with mode 9 of the I-section, and of the J-section, respectively, are close in frequency. Modes for these frequencies have very close nodal locations. Also, the 12th mode of the I-section (see Table 2) was missed in the experimental survey which is indicative of the difficulty of determining the high frequency modes. The fact that only one of the multiple experimental frequencies with close nodal locations (mode 9) is predicted by the finite element model may be attributed to imperfections in lamination and material properties; and/or to geometric nonlinearities which were not incorporated into the finite element model. In Figs. 5(b) and 10(b) bar charts are given for the frequencies obtained by two-dimensional models of the actual and nominal frames along with those of the one-dimensional model.

In Figs. 6 and 11 bar charts are given showing the two decompositions of the complementary strain energies, associated with the different vibration modes, described in the preceding subsection. The ordinates in Figs. 6(a) and 11(a) represent the ratios of U_1/U^c, U_2/U^c and U_3/U^c, and the ordinates in Figs. 6(b) and 11(b) represent the ratios U_{tf}/U^c, U_w/U^c, U_{bf}/U^c for each of the modes.

The mode shapes associated with the first five experimental and analytical frequencies are shown in Figs. 7 and 12. Two views are shown for the deformations associated with each mode: side view and top view. Also shown are the nodal lines of the w' displacement on the top and bottom flanges. As can be seen from Figs. 7 and 12, the deformation patterns associated with higher modes are fairly complex. As mentioned previously, the only experimental nodal lines monitored are those associated with gross in-plane, and gross out-of-plane motions. Generally, good agreement between the finite element and experimental nodal lines is observed in these cases. Other nodal lines, associated with localized deformations are shown only for the finite element solutions.

The sensitivities of the vibration frequencies to the fiber orientation angles of the top flange, web, and bottom flange and skin are depicted in Figs. 8 and 13. The ordinates in Figs. 8 and 13 represent the sensitivity derivatives with respect to the indicated fiber angles. Each of the sensitivity derivatives is normalized by dividing it by the corresponding frequency of vibration. The sensitivities of the vibration frequencies to the material parameters E_L, E_T, G_{LT} and G_{TT} are shown in Figs. 9 and 14. The ordinates in Figs. 9 and 14 represent the sensitivity derivatives with respect to the indicated elastic moduli. Each of the sensitivity derivatives is divided by the corresponding frequency and multiplied by the corresponding elastic modulus. The effects of boundary conditions on the frequencies obtained by the two-dimensional finite element models are shown in Tables 2 and 3.

An examination of the experimental and finite element results (Figs. 5 to 14 and Tables 2 and 3) reveals:

1. Reasonably good correlation is observed between numerical simulation and experiment for the I-section frame (see Fig. 5(b)). The ratios of the first five experimental frequencies to the corresponding finite element ones ranged between 0.92 and 1.02 (see Table 2). For the J-section frame the correlation is not as good (Fig. 10(b)). The corresponding ratios for the first five frequencies were 0.87 to 1.04 (see Table 3).

2. Most of the experimental frequencies for the I-section frame and the J-section frame are between those for the totally and partially clamped supports (with both ϕ_2' and u_1' in the flanges not restrained). This is particularly true for the higher modes. For some of the modes the experimental frequencies are closer to the partially clamped support case (e.g., modes 10, 11 and 12, see Fig. 5(b)). For the I and J-section frames the finite element model predicted only one of the multiple experimental frequencies with close nodal lines (mode 9). The other experimental frequencies were between those for the totally and partially clamped supports (with both ϕ_2' and u_1' in the flanges not restrained, see Fig. 10(b)).

3. The lowest five frequencies obtained by the one-dimensional model are reasonably close to those obtained by the corresponding two-dimensional model. This is particularly true for the J-beam where the errors in the predictions of the one-dimensional model were well below 10% (see Figs. 5(a) and 10(a)).

4. Identification of the modes as in-plane or out-of-plane can best be accomplished by examining the energy components, U_1/U^c and U_2/U^c, associated with the in-plane and out-of-plane forces, respectively (Figs. 6(a) and 11(a)). Also, the error to be expected when using one-dimensional thin-walled beams can be estimated by computing the ratio of the energy associated with the forces neglected in thin-walled beams to the total energy, U_3/U^c (see Figs. 6(a) and 11(a)).

5. The coupling between in-plane and out-of-plane deformations is more pronounced in the J-section than in the I-section frame. As an example, the first twenty modes for the I-section frame had either U_1/U^c or $U_2/U^c \geq 0.75$. On the other hand, only modes 1 to 4, 6, 8 and 10 in the J-section frame had U_1/U^c or $U_2/U^c \geq 0.75$. For the higher modes neither the ratio U_1/U^c nor U_2/U^c was close to 1 (see Figs. 6(a) and 11(a)).

6. For the I-section frame, the contributions to the total energy of the top and bottom flanges far exceeded that of the web for any given mode. The ratio of the strain energy in the web to the total strain energy was less than 0.20 for the first ten modes and less than 0.28 for the succeeding ten modes (see Fig. 6(b)). For the J-section frame the strain energy in the web approached 0.4 of the total energy in some of the modes (see Fig. 11(b)).

7. For the I-section frame, the strain energy of the top flange is the dominant energy in the in-plane deformation modes and the strain energy of the bottom flange (including the skin) dominates for the out-of-plane deformation modes (see Fig. 6(b)).

8. The vibrational response of both the I-section and J-section frames is very sensitive to restraining the u_1 displacements of the flanges (and skin). It is somewhat sensitive to the rotational restraint on ϕ_2, (see Tables 2 and 3). However, it is insensitive to restraining the displacement components u_2, and w', and the rotation ϕ_1,.

9. The vibrational response of the I-section and J-section is more sensitive to variations in the +45°, -45° fiber angles of the top flange than to variations in the 0° or 90° fiber angles. The variations in the 0° and 90° fibers of the web and the bottom flange have a noticeable effect on some of the modes, but their effect is generally less than that of the 45°, -45° fibers (see Figs. 8 and 13). The vibrational response is also more sensitive to variations in the elastic moduli E_L and G_{LT} than to any of the other material coefficients (see Figs. 9 and 14).

10. The sensitivity of the vibration frequencies with respect to variations in both E_L and G_{LT} is almost the same for all the modes (see Figs. 9 and 14). This may be attributed to the quasi-isotropic lamination used for both the flanges and the web. It suggests the feasibility of replacing the quasi-isotropic composite, in the one-dimensional thin-walled beam model, by an equivalent isotropic material, as was done in the present study.

Comments on Sources of Errors

Sources of Errors

The determination of natural frequencies and modes from vibration tests and numerical models involves numerous possible sources of discrepancies or errors which are related to mechanical and equipment limitations as well as to theoretical and physical assumptions. The errors in vibration tests include inexact equipment calibration, excessive noise, manufacturing variations, incorrect transducer locations and operation in a region of nonlinearity of the response. Numerical modeling errors can be attributed to inaccuracies in estimated material properties and insufficient modeling detail. In the present study care was exercised in collecting and recording the vibration test data, and in the selection of the numerical model. However, nominal material properties and layups (fiber orientation of the different layers) were used in the numerical model. The sensitivity analysis helped in identifying the material and lamination parameters that need to be accurately determined.

Concluding Remarks

A detailed study was made of the effects of variations in lamination and material parameters on their vibrational characteristics of thin-walled composite frames. The structures considered are semicircular, thin-walled frames with I and J cross sections. The flanges, web and skin of the stiffeners have quasi-isotropic laminations with fiber orientation being combinations of ± 45°, 0° and 90° layers. Two computational models are used for predicting the vibrational characteristics. In the first model, the flanges and webs of the stiffeners were modeled by using two-dimensional shell (and plate) finite elements. The second model was a finite element discretization of the one-dimensional Vlasov's-type thin-walled beam theory. A mixed formulation was used with the fundamental unknowns consisting of both the generalized displacements and stress resultants (or internal forces) in the frame. The frequencies and modes predicted by the computational models are compared with those obtained from experiments. A detailed study was made of the sensitivity of the vibrational response to variations in the fiber orientation, material properties of the individual layers, and boundary conditions. On the basis of this study the following conclusions are justified:

1. For some of the higher vibration modes the experimental frequencies for thin-walled frames are generally between those for the totally and partially clamped supports.

2. Identification of the modes as in-plane or out-of-plane can best be accomplished by examining the energy components associated with the in-plane and out-of-plane forces. Also, the minimum error to be expected when using one-dimensional thin-walled beams can be estimated by computing the ratio of the energy associated with the forces neglected in thin-walled beams to the total energy.

3. For quasi-isotropic composite frames the vibration frequencies, associated with the lower modes, can be accurately predicted by isotropic one-dimensional beam model (with effective elastic moduli). The accuracy of predictions is

dependent on the cross-sectional distortions during the beam deformations. As the cross-sectional distortions increase, the degradation of accuracy becomes more pronounced.

4. The vibrational response of thin-walled semicircular frames is very sensitive to restraining the displacement component of the flanges along the length of the frame. It is somewhat sensitive to the restraint on the associated rotational component. However, it is less sensitive to restraining the other displacement and rotation components.

5. The vibrational response of thin-walled composite frames with quasi-isotropic laminations is more sensitive to variations in the +45°, -45° fiber angles of the top flange than to variations in the 0° or 90° fiber angles. Variations in the 0° and 90° fibers of the web and the bottom flange have a noticeable effect on some of the modes, but their effect is generally less than that of the 45°, -45° fibers. The vibrational response is also more sensitive to variations in the material coefficients E_L and G_{LT} than to all other coefficients.

6. The sensitivity of the vibration frequencies with respect to variations in both E_L and G_{LT} is almost the same for all the modes. This may be attributed to the quasi-isotropic lamination used for both the flanges and the web. It suggests the feasibility of replacing the quasi-isotropic composite by an equivalent isotropic material in the one-dimensional thin-walled beam analysis, as was done in the present study.

References

1. Boitnott, R. L., Fasanella, E. L., Calton, L. E. and Carden, H. D.: Impact Response of Composite Fuselage Frames. *Technical Paper Series* No. 891009, The Engineering Society for Advancing Mobility, Land, Sea, Air, and Space, Warrendale, PA, April 1987.

2. Boitnott, R. L. and Fasanella, E. L.: Impact Evaluation of Composite Floor Sections. *SAE Technical Paper Series* No. 891018, The Engineering Society for Advancing Mobility, Land, Sea, Air, and Space, Warrendale, PA, April 1989.

3. Collins, J. S. and Johnson, E. R.: Static and Free-Vibrational Response of Semi-Circular Graphite-Epoxy Frames with Thin-Walled Open Sections. Report CCMS-89-21, Center for Composite Materials and Structures, Virginia Polytechnic Institute and State University, Blacksburg, VA, October 1989.

4. Chandra, R., Ngo, H. and Chopra, I.: Experimental Study of Thin-Walled Composite Beams. *Proceedings of the National Technical Specialists' Meeting on Advanced Rotorcraft Structures*, Oct. 25-27, 1988, Williamsburg, VA, American Helicopter Society, 1988.

5. Vlasov, V. Z. (Y. Schechtman, transl.): *Thin-Walled Elastic Beams*. Israel Program for Scientific Translations, 1961.

6. Gjelsvik, A.: *The Theory of Thin Walled Bars*. John Wiley & Sons, Ltd., 1981.

7. Nowinski, J. L.: Theory of Thin-Walled Bars. *Applied Mechanics Surveys*, H. Norman Abramson, Harold Liebowitz, John M. Crowley and Stephen Juhasz, eds., Spartan Books, 1966, pp. 325-338.

8. Panovko, Ya. G.; and Beilin, E. A.: Thin-Walled Beams and Systems Consisting of Thin-Walled Beams. *Structural Mechanics in the USSR - 1917-1967*, I. M. Rabinovich, ed., Moscow Publ. House, 1969, pp. 75-98 (in Russian).

9. Hasan, S. A. and Barr, A. D. S.: Linear Vibration of Thin-Walled Beams of Equal Angle-Section. *J. Sound & Vibration*, vol. 32, Jan. 1974, pp. 3-23.

10. Vermishian, G. B.: Torsion of a Viscoelastic Prismatic Composite Rod Under the Action of a Vibrational Load. *Akademiia Nauk Armianskoi SSR, Izvestiia, Mekhanika*, vol. 27, no. 1, 1974, pp. 48-62 (in Russian).

11. Rao, C. K.: Nonlinear Torsional Vibrations of Thin-Walled Beams of Open Section. *J. Applied Mechanics*, vol. 42, March 1975, pp. 240-242.

12. Vasilenko, N. V. and Trivailo, P. M.: Vibration of Thin-Walled Rods with Open Profile of Material with Nonlinear Hysteresis. *Problemy Prochnosti*, Nov. 1979 pp. 72-76 (in Russian) (English translation in *Strength of Materials*, vol. 11, no. 11, July 1980, pp. 1279-1285).

13. Narayanan, S., Mallik, A. K. and Verma, J. P.: Free Vibration of Thin-Walled Open Section Beams with Unconstrained Damping Treatment. *J. Appl. Mech.*, vol. 48, March 1981, pp. 169-173.

14. Ali, S. A.: Stability of Bending-Torsional Vibrations of Curved Thin-Walled Beams. *J. Sound & Vib.*, vol. 95, Aug. 1984, pp. 341-350.

15. Gupta, R. K., Venkatesh, A. and Rao, K. P.: Finite Element Analysis of Laminated Anisotropic Thin-Walled Open-Section Beams. *Composite Structures*, vol. 3, 1985, pp. 19-31.

16. Potiron, A., Gay, D., Czekajski, C. and LaRoze, S.: Limitation of Simplified Hypotheses for the Prediction of Torsional Oscillations for Thin-Walled Beams. *J. Vibration, Acoustics, Stress & Reliability in Design*, vol. 107, Jan. 1985, pp. 117-122.

17. Ruckschloss, J. and Tesar, A.: Transfer Matrix Formulation for Solution of Torsion-Bending Vibration of Beams with Thin-Walled Cross Section. *Acta Technica CSAV*, vol. 30, no. 5, 1985, pp. 524-538.

18. Wekezer, J. W.: Free Vibrations of Thin-Walled Bars with Open Cross Sections. *J. Eng. Mech.*, vol. 113, no. 10, Oct. 1987, pp. 1441-1453.

19. Rehfield, L. W., Hodges, D. H. and Atilgan, A. R.: Some Considerations on the Nonclassical Behavior of Thin-Walled Composite Beams. *National Technical Specialists' Meeting on Advanced Rotorcraft Structures, Proc.*, Oct. 25-27, 1988, Williamsburg, VA, American Helicopter Society, 1988.

20. Stemple, A. D. and Lee, S. W.: Finite-Element Model for Composite Beams with Arbitrary Cross-Sectional Warping. *AIAA Journal*, vol. 26, Dec. 1988, pp. 1512-1520.

21. Bishop, R. E. D., Cannon, S. M. and Miao, S.: On Coupled Bending and Torsional Vibration of Uniform Beams. *J. Sound & Vibration*, vol. 131, June 1989, pp. 457-464.

22. Teh, K. K. and Huang, C. C.: The Effects of Fibre Orientation on Free Vibrations of Composite Beams. *J. Sound & Vibration*, vol. 69, March 1980, pp. 327-337.

23. Bank, L. C. and Kao, C. H.: The Influence of Geometric and Material Design Variables on the Free Vibration of Thin-Walled Composite Material Beams. *Journal of Vibration, Acoustics, Stress and Reliability in Design*, vol. 111, July 1989, pp. 290-297.

24. Noor, A. K., Carden, H. D. and Peters, J. M.: *Free Vibrations of Thin-Walled Semicircular Graphite-Epoxy Composite Frames*. NASA TP (to appear).

25. Noor, A. K., Peters, J. M. and Min, B. J.: *Mixed Finite Element Models for Free Vibrations of Thin-Walled Beams*. NASA TP-2868, Feb. 1989.

26. Noor, A. K. and Andersen, C. M.: Mixed Models and Reduced/Selective Integration Displacement Models for Nonlinear Shell Analysis. *Int. J. Numer. Methods Eng.*, vol. 18, no. 10, Oct. 1982, pp. 1429-1454.

27. Noor, A. K. and Peters, J. M.: Mixed Models and Reduced Selective Integration Displacement Models for Vibration Analysis of Shells. *Hybrid and Mixed Finite Element Methods*, S. N. Atluri, R. H. Gallagher and O. C. Zienkiewicz, eds., John Wiley & Sons, 1983, pp. 537-564.

28. Nelson, R. B.: Simplified Calculation of Eigenvector Derivatives. *AIAA Journal*, vol. 14, 1976, pp. 1201-1205.

29. Jones, R. M.: *Mechanics of Composite Materials*. Hemisphere Pub. Co., New York, 1975.

30. Coyette, J. P.: An Improved Subroutine for the Estimation of Torsional Properties of Thin-Walled Open Cross Sections. *Eng. Comput.*, vol. 4, no. 3, Sept. 1987, pp. 240-242.

31. Chen, J. C. and Garba, J. A.: Matrix Perturbation for Analytical Model Improvement. *Proceedings of the AIAA/ASME/ASCE/AHS 20th Structures, Structural Dynamics and Materials Conference, A Collection of Technical Papers on Dynamics and Loads*, April 4-6, 1979, St. Louis, MO, pp. 428-436.

32. Crawley, E. F. and Jensen, D. W.: Frequency Determination Techniques for Cantilevered Plates with Bending-Torsion Coupling. *AIAA Journal*, vol. 22, March 1984, pp. 415-420.

33. Ewins, D. J.: *Modal Testing: Theory and Practice*. Research Studies Press, John Wiley & Sons, Ltd., 1984.

34. Falco, M. and Gasparetto, M.: Flexural-Torsional Vibrations of Thin-Walled Beams. *Meccanica*, vol. 8, Sept. 1973, pp. 181-189.

35. Arruda, J. R. de F.; and Santos, J. M. C. dos: Model Adjusting of Structures with Mechanical Joints Using Modal Synthesis. *Proceedings of the Seventh International Modal Analysis Conference*, Jan. 30-Feb. 2, 1989, Las Vegas, NV, vol. II, Society for Experimental Mechanics, Inc., Bethel, CT, 1989, pp. 850-856.

36. Baruch, M.: Optimal Correction of Mass and Stiffness Matrices Using Measured Modes. *AIAA Journal*, vol. 20, no. 11, Nov. 1982, pp. 1623-1626.

37. Berman, A.: Mass Matrix Correction Using an Incomplete Set of Measured Modes. *AIAA Journal*, vol. 17, no. 10, Oct. 1979, pp. 1147-1148.

38. Berman, A. and Wei, F. S.: *Automated Dynamic Analytical Model Improvement*. NASA CP-3452, July 1981.

39. Berman, A. and Nagy, E. J.: Improvement of a Large Analytical Model Using Test Data. *AIAA Journal*, vol. 21, no. 8, Aug. 1983, pp. 1168-1173.

40. Grossman, D. T.: An Automated Technique for Improving Modal Test/Analysis Correlation. *Proceedings of the AIAA/ASME/ASCE/AHS 23rd Structures, Structural Dynamics and Materials Conference, Part 2, A Collection of Technical Papers*, May 10-12, 1982, New Orleans, LA, pp. 68-76.

41. Jensen, D. W. and Crawley, E. F.: Comparison of Frequency Determination Techniques for Cantilevered Plates with Bending-Torsion Coupling. *Proceedings of the AIAA/ASME/ASCE/AHS 24th Structures, Structural Dynamics and Materials Conference, Part 2, A Collection of Technical Papers*, May 2-4, 1983, Lake Tahoe, NV, pp. 737-743.

42. Kabe, A. M.: Stiffness Matrix Adjustment Using Mode Data. *AIAA Journal*, vol. 23, no. 9, Sept. 1985, pp. 1431-1436.

43. Martinez, D. R. and Miller, A. K. (eds.): *Combined Experimental/Analytical Modeling of Dynamic Structural Systems*. Joint ASCE/ASME Mechanics Conference, Albuquerque, NM, June 24-26, 1985, ASME Publication.

44. Wei, F. H.: Stiffness Matrix Correction From Incomplete Test Data. *AIAA Journal*, vol. 18, no. 10, Oct. 1980, pp. 1274-1275.

45. Zhirohowski-Koscia, K.: *Thin-Walled Beams - From Theory to Practice.* Crosby Lockwood & Son, Ltd., 1967.

APPENDIX A - Symbols

A_{11}	extensional stiffness of the laminate (flanges or web) in the x_1-direction
A_{33}	in-plane shear stiffness of the laminate
c_i	multipliers (see Eqs. 5 and 7)
E, G	effective Young's and shear moduli of the equivalent isotropic material, respectively
E_L, E_T	elastic moduli of the individual layers of the laminate (flanges or web) in the direction of fibers and normal to it, respectively
$\|F\|$	matrix of linear flexibility coefficients for an individual element
G_{LT}, G_{TT}	shear moduli in the plane of fibers and normal to it, respectively
$\{H\}$	vector of stress resultant (or internal force) parameters
h	total thickness of the laminate
$\overset{*}{\|K\|}$	generalized stiffness matrix for an individual element (see Eqs. 3)
M_y, M_z, M_t	bending and twisting moments in the one-dimensional beam model
M_1, M_2, M_{12}	bending stress resultants in the two-dimensional model
$\|M\|$, $\overset{*}{\|M\|}$	consistent and generalized mass matrices for an individual element (see Eqs. 3)
N_1, N_2, N_{12}	extensional stress resultants in the two-dimensional model
N_x	axial force in the one-dimensional beam model
Q_y, Q_z	transverse shear forces in the one-dimensional beam model
Q_1, Q_2	transverse shear stress resultants in the two-dimensional model
R	radius of curvature of the centerline of the frame (used in one-dimensional beam model)
R_1	outer radius of curvature of the frame (see Fig. 1)
U^c	total complementary strain energy of the frame
U_{tf}, U_w, U_{bf}	contributions of the top flange, web and bottom flange (including the skin) to the total complementary strain energy
U_1, U_2	complementary strain energy components associated with in-plane and out-of-plane forces, respectively
U_3	complementary strain energy component associated with the forces neglected in the one-dimensional beam model
u, v, w	displacement components in coordinate directions for the one-dimensional beam model
u_1, u_2, w	displacement components of the two-dimensional model in the x_1, x_2, x_3 coordinate directions
u_1', u_2', w'	displacement components of the two-dimensional model in the x_1', x_2', x_3' coordinate directions
$\{X\}$	vector of nodal displacements
x_1, x_2, x_3	local orthogonal coordinate system used in conjunction with the two-dimensional model (for each of the web and the two flanges)
$\{Z\}$	vector of element degrees of freedom
$\overset{*}{\{Z\}}$	particular solution (see Eqs. 5 and 6)
θ	fiber orientation of individual layers
λ_i	lamination and material parameters
ρ	mass density of material
ν_{LT}	major Poisson's ratio of the individual layers
ϕ_1, ϕ_2	rotation components of the two-dimensional model referred to the local coordinate system x_1, x_2
ϕ_1', ϕ_2', ϕ_3'	rotation components of the two-dimensional model referred to the global coordinate system x_1', x_2', x_3'
ω	frequency of vibration
∂	$\equiv d/dx$
Subscripts:	
1D	one-dimensional finite element model
2D	two-dimensional finite element model
s	shear center
Superscripts:	
t	matrix transposition

Table I.- Decomposition of total complementary energy, U^c into components.

Energy Components	Associated stress resultant (see Fig. 2)		Comments
	Web	Flanges and Skin	
U_1	N_1, N_{12}	N_1, M_1, Q_1	in plane response quantities
U_2	M_1, M_{12}, Q_1	$N_{12}, M4$	out-of-plane response quantities
U_3	N_2, M_2, Q_2		response quantities neglected in one-dimensional model

$U^c = U_1 + U_2 + U_3$

Table 2 - Effect of boundary conditions on the frequencies (in hertz) obtained by the two-dimensional finite element model for the I-section frame

Mode	Totally Clamped Model	Partially clamped model (with the following generalized displacements unrestrained) ϕ_2'	ϕ_2', ϕ_3'	u_1' in the flanges	u_1' in the flanges & ϕ_2'	Experiment
1	9.201	9.001 (0.978)	9.001 (0.978)	6.788 (0.738)	6.632 (0.721)	9.200
2	31.86	31.06 (0.975)	31.06 (0.975)	18.11 (0.568)	17.87 (0.561)	29.70
3	37.52	37.37 (0.996)	37.37 (0.996)	34.17 (0.911)	33.56 (0.889)	35.90
4	73.85	71.82 (0.973)	71.81 (0.972)	38.09 (0.516)	37.69 (0.510)	66.60
5	81.34	81.03 (0.996)	81.03 (0.996)	74.30 (0.913)	73.44 (0.903)	78.10
6	133.9	130.1 (0.972)	130.1 (0.972)	75.56 (0.564)	74.14 (0.554)	119.0
7	149.2	148.6 (0.996)	148.6 (0.996)	129.6 (0.869)	128.1 (0.858)	145.0
8	203.3	198.1 (0.974)	198.1 (0.974)	139.8 (0.688)	137.4 (0.676)	193.0
9	226.5	25.6 (0.996)	225.6 (0.996)	199.3 (0.880)	196.9 (0.870)	216.0 223.0
10	281.9	275.2 (0.976)	275.2 (0.976)	214.2 (0.760)	210.9 (0.748)	260
11	320.6	319.3 (0.996)	319.3 (0.996)	268.0 (0.836)	264.9 (0.826)	309
12	349.8	342.3 (0.979	342.3 (0.979)	305.1 (0.872)	300.7 (0.860)	*(Missed)*
13	419.1	412.6 (0.985)	412.6 (0.985)	343.0 (0.819)	339.0 (0.809)	401.0

Table 3 - Effect of boundary conditions on the frequencies (in hertz) obtained by the two-dimensional finite element model for the J-section frame

Mode	Totally Clamped Model	Partially clamped model (with the following generalized displacements unrestrained) ϕ_2'	ϕ_2', ϕ_3'	u_1' in the flanges	u_1' in the flanges & ϕ_2'	Experiment
1	11.53	11.24 (0.975)	11.24 (0.975)	8.488 (0.736)	8.408 (0.729)	11.60
2	36.87	36.64 (0.994)	36.64 (0.994)	22.41 (0.608)	22.37 (0.607)	32.10
3	39.81	38.80 (0.975)	38.79 (0.974)	32.77 (0.823)	32.18 (0.808)	37.00
4	79.22	78.99 (0.997)	78.99 (0.997)	48.32 (0.610)	47.94 (0.605)	69.00
5	91.41	88.81 (0.972)	88.78 (0.971)	72.64 (0.795)	71.68 (0.784)	79.00
6	143.9	143.5 (0.997)	143.5 (0.997)	96.58 (0.671)	95.35 (0.663)	126.0
7	168.1	163.6 (0.973)	163.5 (0.973)	134.4 (0.800)	132.9 (0.790)	145.0
8	214.1	213.4 (0.997)	213.4 (0.997)	167.2 (0.781)	165.0 (0.770)	191.0
9	263.0	256.9 (0.977)	256.8 (0.976)	206.5 (0.785)	204.3 (0.770)	221.0 229.0 247.0
10	297.6	296.2 (0.995)	296.2 (0.995)	251.5 (0.845)	248.3 (0.834)	266.0
11	368.2	361.2 (0.981)	361.1 (0.981)	298.7 (0.811)	295.5 (0.803)	339.0
12	382.8	380.3 (0.993)	380.3 (0.993)	336.7 (0.880)	332.8 (0.869)	347.0

Note: Numbers between parentheses refer to the ratios of the partially clamped to the totally clamped model frequencies.

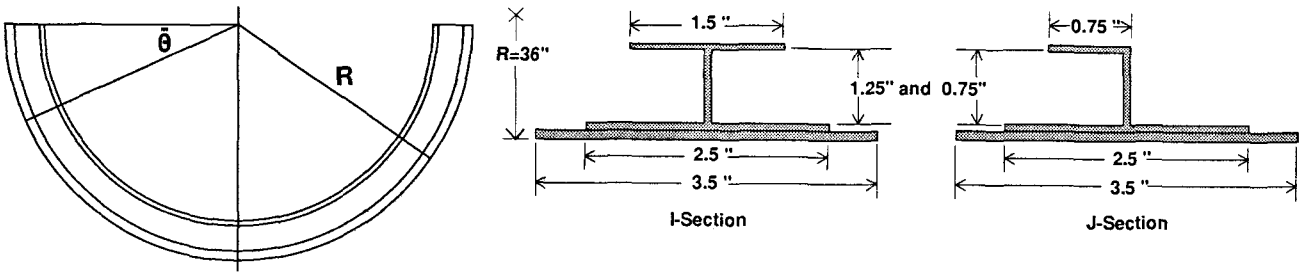

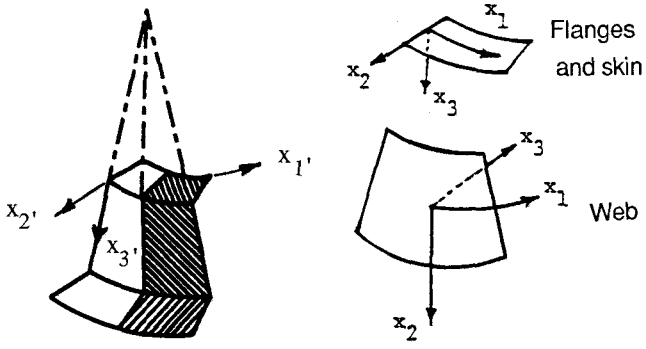

Material Properties

$E_L = 2.0 \times 10^7$ psi

$E_T = 1.7 \times 10^6$ psi

$G_{LT} = 9.3 \times 10^5$ psi

$G_{TT} = 6.51 \times 10^5$ psi

$\upsilon_{LT} = 0.38$

$\rho = 0.058$ lb/in.^{3}

Nominal layer thickness = 0.005 in.

Fiber Orientation

NL = 8 : $[\pm 45/0/90]_s$

NL = 16 : $[\pm 45/0/90]_{2s}$

Figure 1.- Thin-walled composite frames and coordinate systems used in present study.

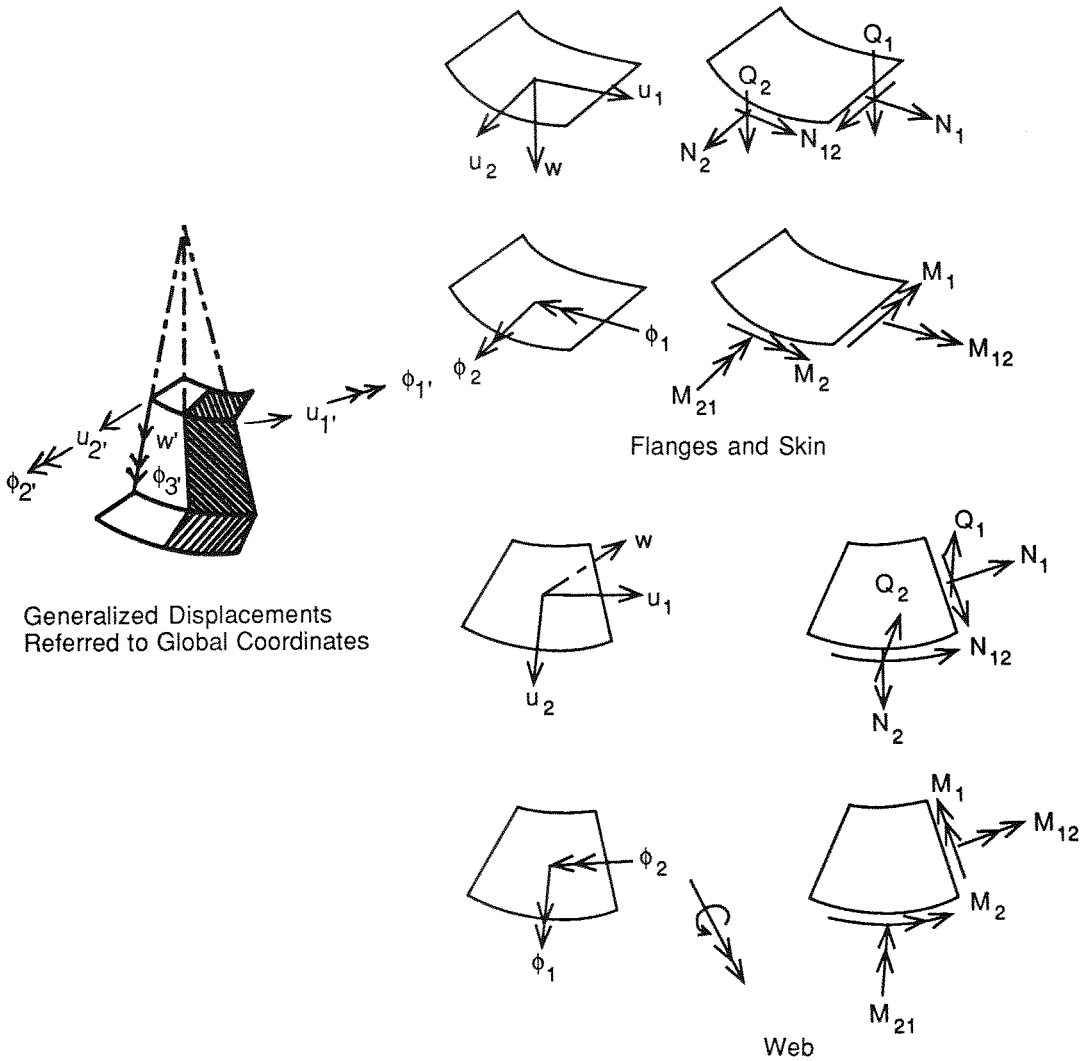

Figure 2.- Sign convention for generalized displacements and stress resultants in two-dimensional model.

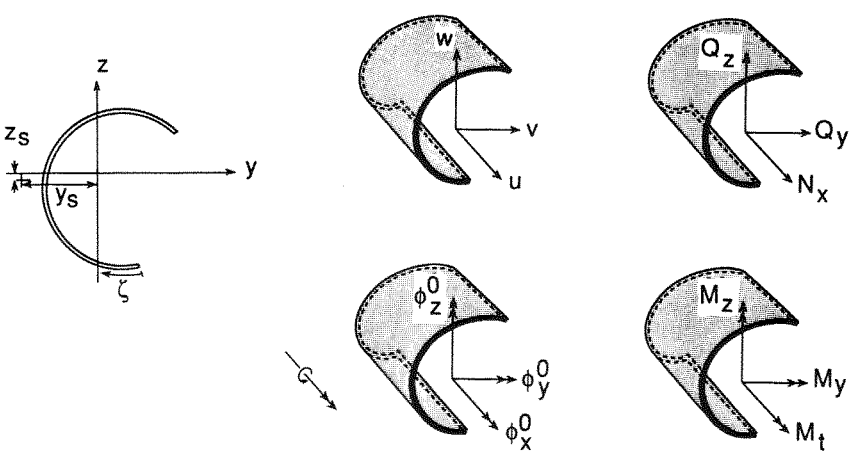

Figure 3.- Sign convention for generalized displacements and stress resultants for one-dimensional model.

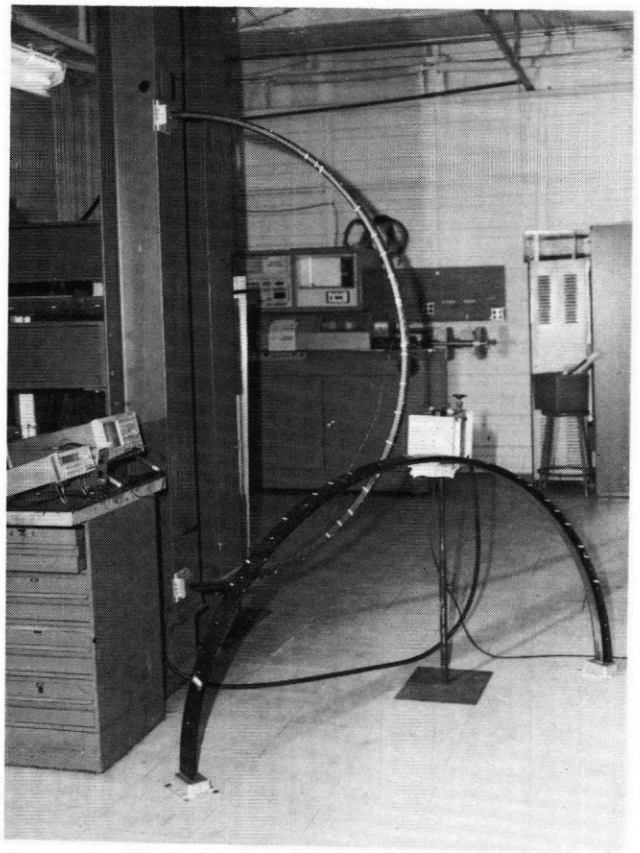

Figure 4.- Photograph of thin-walled semi-circular graphite-epoxy specimens and experimental equipment.

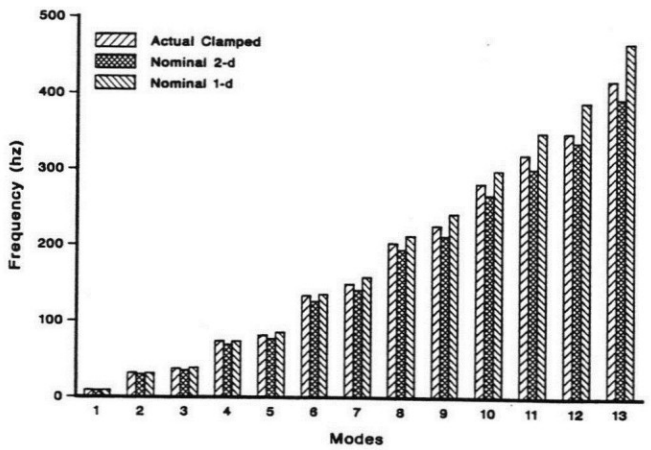

(a) Two-dimensional and one-dimensional beam model results.

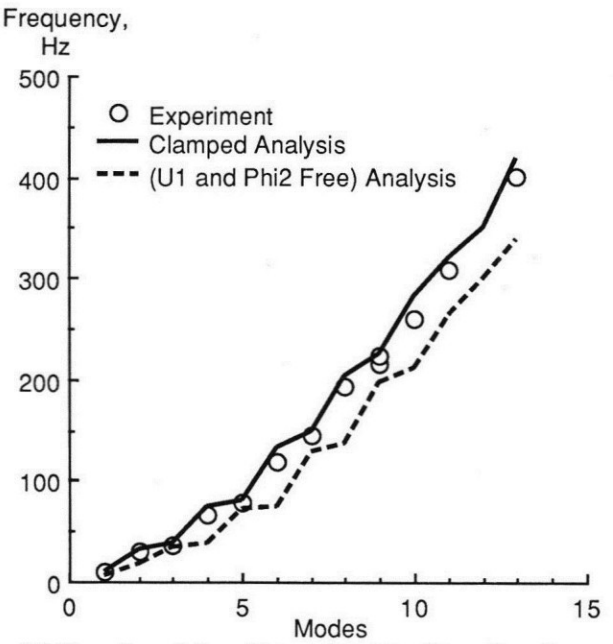

(b) Experimental and bounding two-dimensional model results.

Figure 5.- Comparison of finite element and experimental frequencies for the thin-walled composite frame with I cross-section.

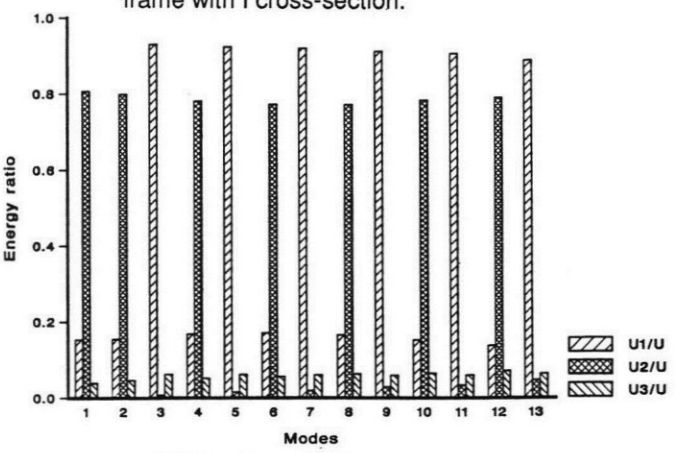

(a) U_1, U_2, and U_6 components.

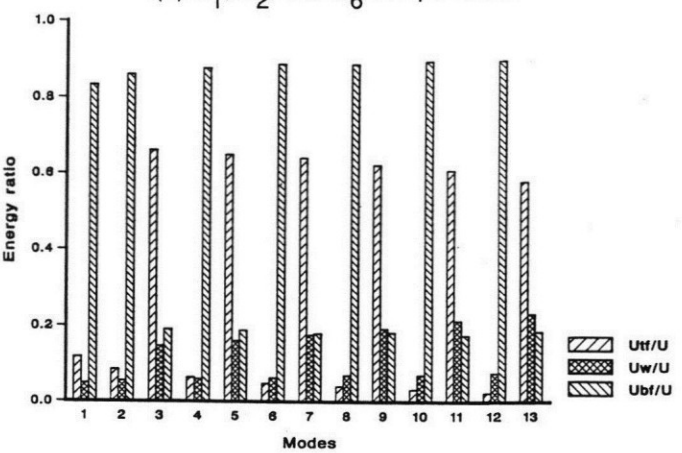

(b) U_{tf}, U_w, and U_{bf} components.

Figure 6. - Energy components in the different vibration modes of the thin-walled composite frame with I cross-section.

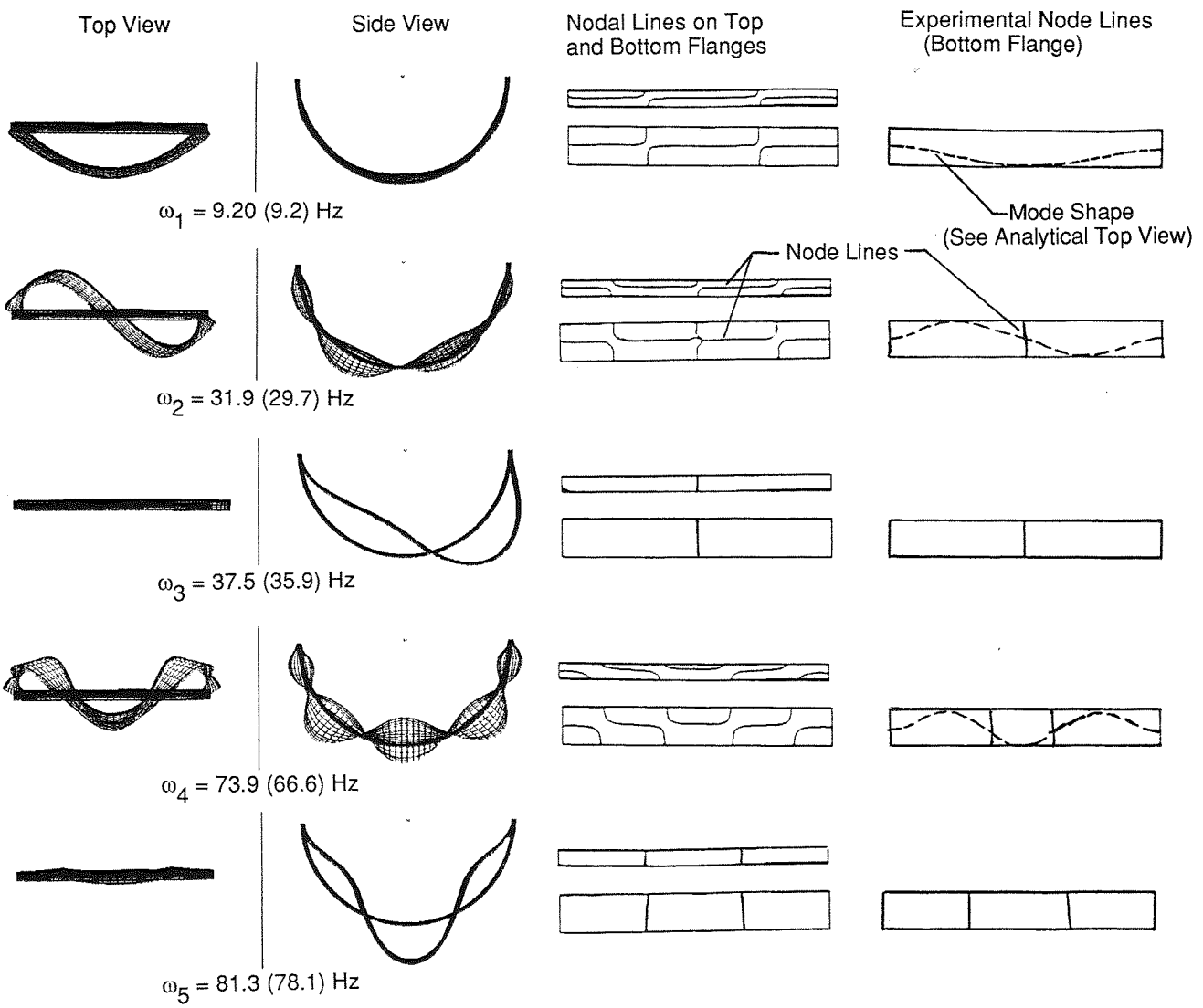

Figure 7.- Mode shapes associated with the lowest five frequencies for the thin-walled composite frame with I cross-section. Parentheses are experimental frequencies. Others are clamped finite element model results.

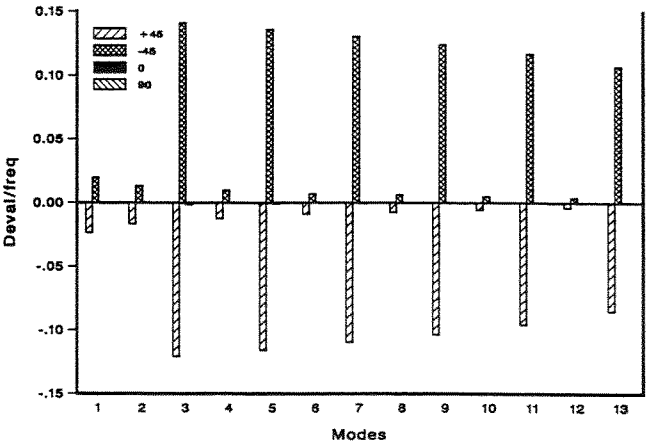

(a) Top flange.

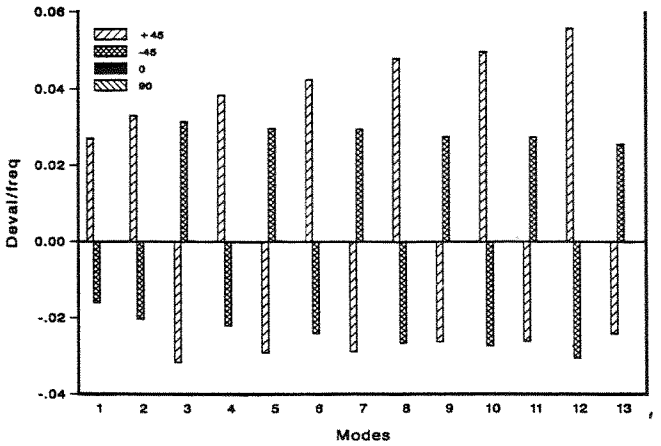

(b) Web.

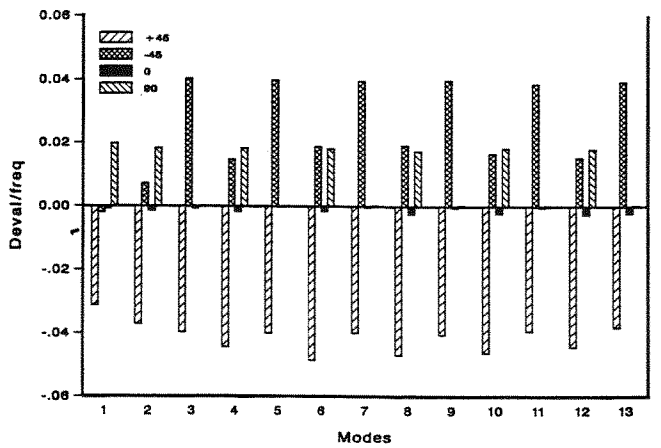

(c) Bottom flange and skin.

Figure 8.- Sensitivity of vibration frequencies to fiber orientation angle in the flanges and web of the thin-walled composite frame with I cross-section.

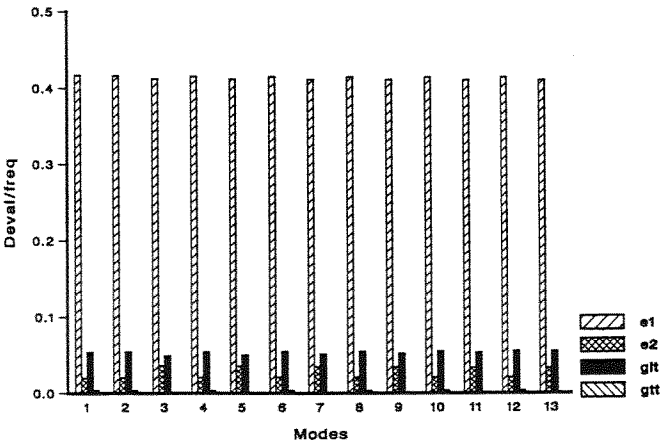

Figure 9.- Sensitivity of vibration frequencies to variations in material characteristics of the thin-walled composite frame with I cross-section.

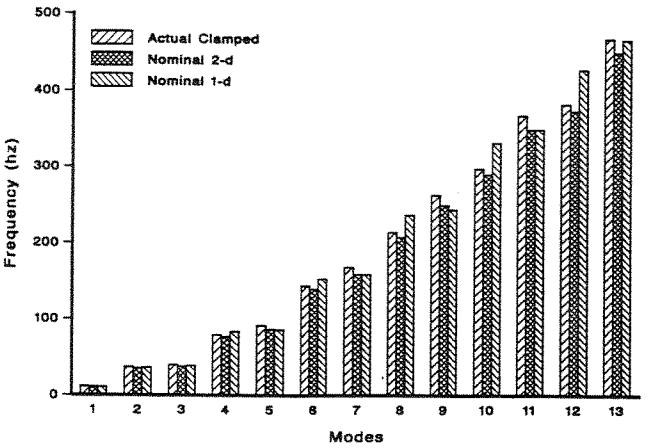

(a) Two-dimensional and one-dimensional beam model results.

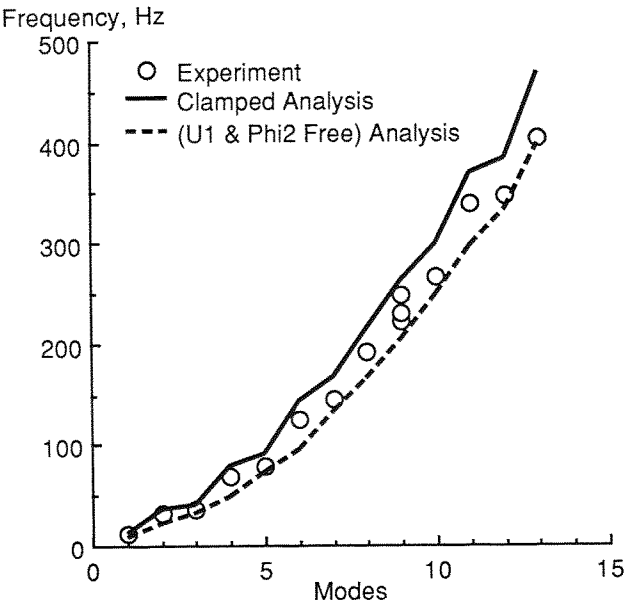

(b) Experimental and bounding two-dimensional model results.

Figure 10.- Comparison of finite element and experimental frequencies for the thin-walled composite frame with J cross-section.

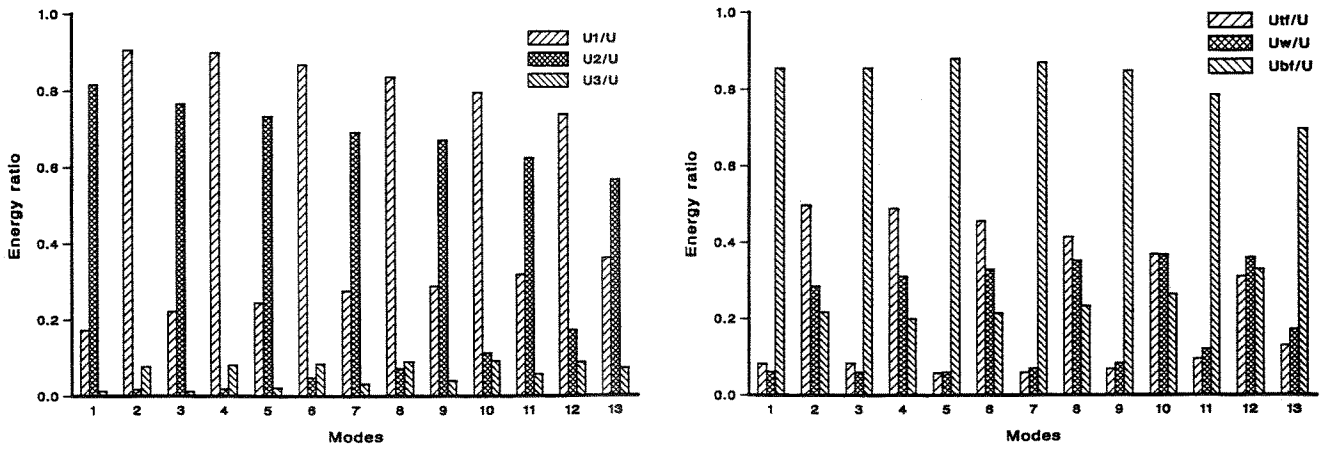

(a) U_1, U_2, and U_3 comoponents.

(b) U_{tf}, U_w, and U_{bf} components.

Figure 11.- Energy components in the different vibration modes of the thin-walled composite frame with J cross-section.

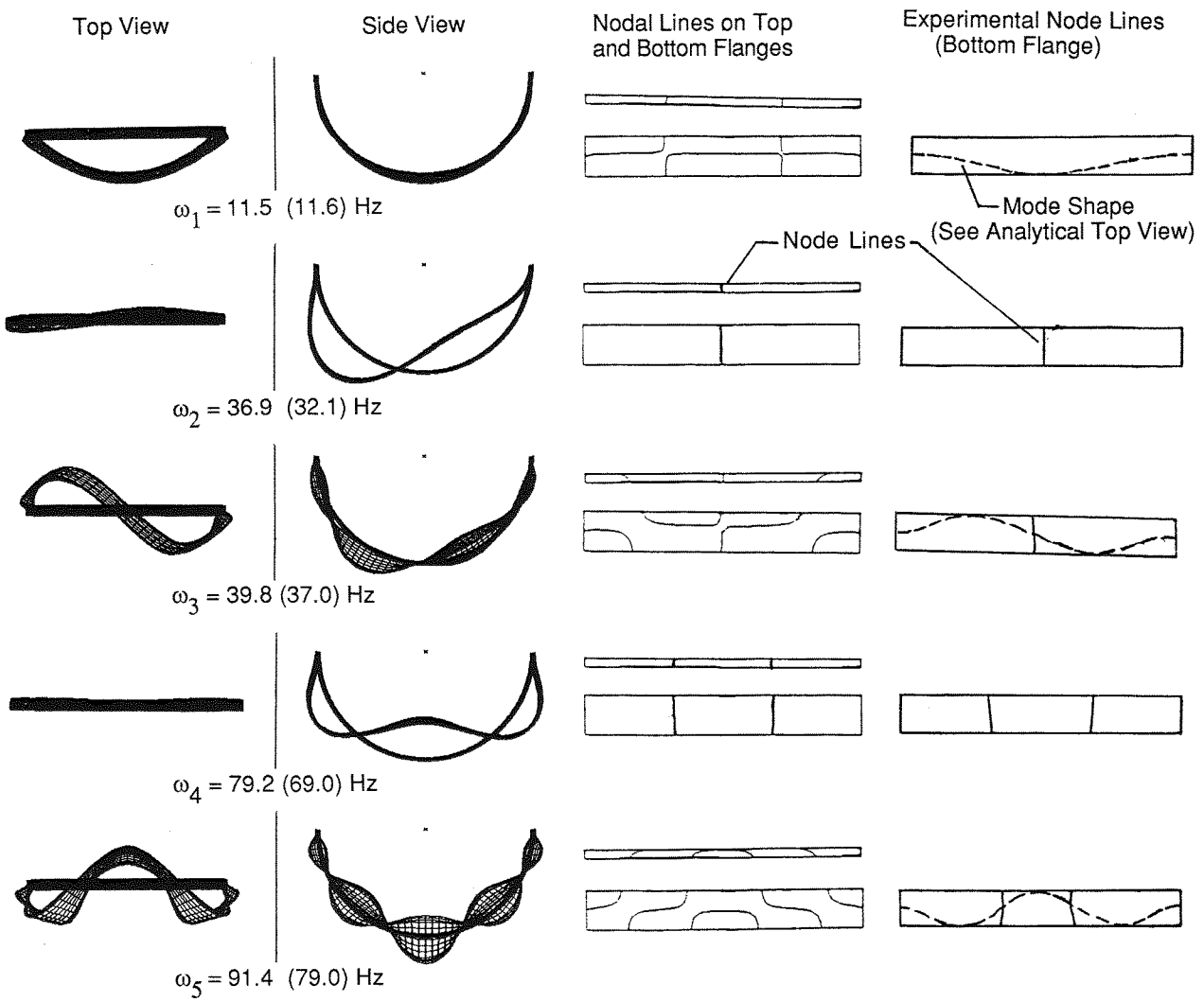

Figure 12.- Mode shapes associated with the five lowest frequencies of the thin-walled composite frame with J cross-section. Parentheses are experimental frequencies. Others are clamped finite element model results.

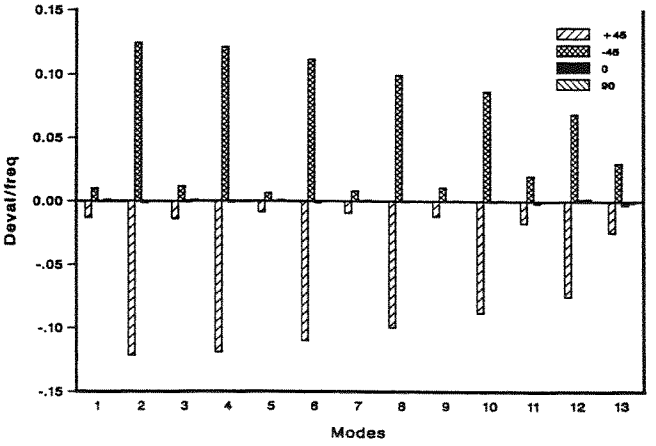

(a) Top flange.

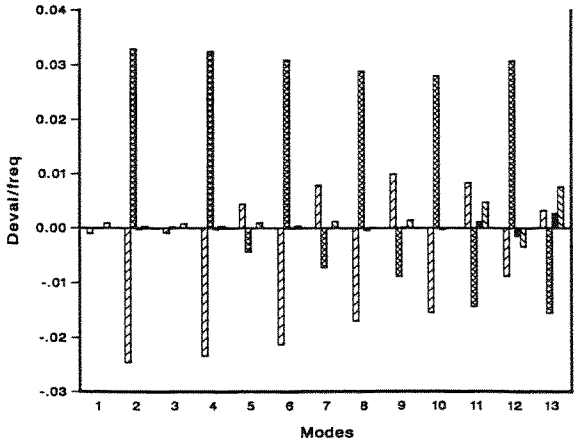

(b) Web.

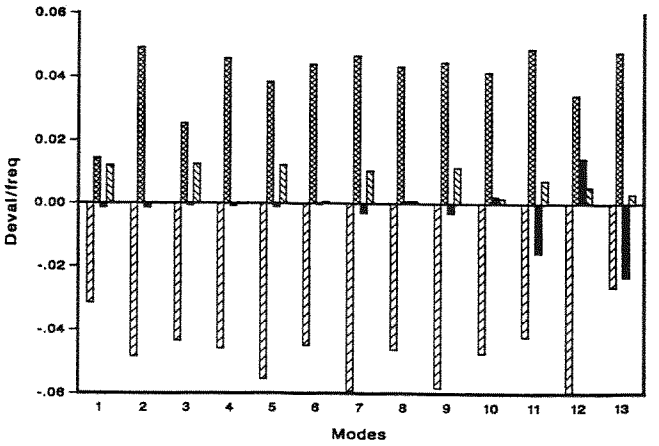

(c) Bottom flange and skin.

Figure 13.- Sensitivity of vibration frequencies to variations in the fiber orientation angle in the flanges and web of the thin-walled composite frame with J cross-section.

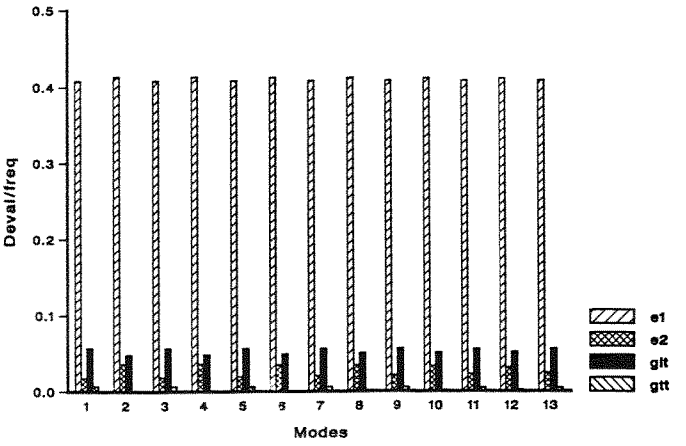

Figure 14.- Sensitivity of vibration frequencies to variations in the material characteristics of the thin-walled composite frame with J cross-section.